Materials International
Open Access Journal (ISSN: 2668-5728)

Article
Volume 6, Issue 2, 2024, 19
https://doi.org/10.33263/Materials62.019

Exploring Fish Scale-Derived Hydroxyapatite Doped with NaCl for Enhanced Bone Tissue Regeneration

Magapu Solomon Sudhakar [1], Aakriti Aggarwal [2], Salama Alsheriqi [1], Balqis Alshabibi [1], Noor Salim Said AlBuraik [1], Basma Ali Albadri [1], Bushra Mohammed Saif Al-Breiki [1], Mahesh Kumar Sah [2,*]

[1] Applied Biotechnology Department, University of Technology and Applied Sciences-Sur, Sur, P.O.484, P.C.411., Oman
[2] Department of Biotechnology, Dr. B R Ambedkar National Institute of Technology, Jalandhar 144011, Punjab, India
* Correspondence: sahmk@nitj.ac.in;

Scopus Author ID 49662349800
Received: 22.04.2023; Accepted: 28.01.2024; Published: 10.06.2024

Abstract: Using raw fish scales as a hydroxyapatite (HAp) source for tissue engineering applications is gaining attention. In this study, hydroxyapatite was derived from Catla (*Catla catla*) and Tilapia (*Oreochromis niloticus*) fish species to develop load-bearing biomaterials required for bone tissue ingrowth. The sample groups were labeled as S, T, and C (for standard HAp, Tilapia-derived HAp, and Catla-derived HAp, respectively). However, naturally derived HAp scaffolds are limited by low physico-mechanical stability. Therefore, this study aimed to enhance their physical properties by doping with Sodium chloride. FTIR analysis revealed peak positions for $CaCO_3^{2-}$ and PO_4^{2-} groups present in all samples at around 712 cm^{-1}, 1407 cm^{-1}, and 1036 cm^{-1}. The XRD studies indicated prominent 2θ values (at 26, 32, 39, 49, and 64) corresponding to standard HAp powder, confirming its presence and crystallinity in all samples. Elemental analysis with EDS confirmed the presence of Ca and P in the ratio of almost 1.8:1 (wt%) in all sample groups. The tailored material developed from fish scales showed potential in supporting bone tissue regeneration, as suggested by biorelevant studies. These findings suggest that fish scale-derived HAp could be a promising resource for developing load-bearing biomaterials for bone tissue engineering applications.

Keywords: fish scales; hydroxyapatite; biomaterials; doping; bone tissue.

1. Introduction

The occurrence of bone lesions and fractures pose as one of the most common large organ injuries in humans, [1] also leading to traumatic complications, especially in the aged population [2]. As the second most transplanted tissue, diseased or injured bones demand numerous substitutes [3]. This is typically performed directly by the patient or from appropriate donors. The dearth of tissue supplies, morbidity at the donor site, and incompatibility make these procedures only effective for smaller-size abnormalities [4]. Treatment of bone defects through the multidisciplinary field of tissue engineering is the newest choice [5], which involves optimum scaffold interactions with the cells and other regulatory factors to mimic the target tissue [6,7] effectively. The physicochemical characteristics of the scaffolds serve as essential requirements for achieving desired cell growth. This necessitates that materials and bone tissue engineering work synergistically to develop biomaterial alternatives, along with controlled architecture for bone remodeling [8].

Hydroxyapatite is being extensively studied and explored in this field due to its presence in the natural bone [9] and its ability to activate osteoblast proliferation and mesenchymal stem cell differentiation by increasing the concentration of calcium ions at the local site [10]. It is chemically synthesized [11,12] or obtained from natural sources, such as bovine bone [1]. The major hindrances to these methods are high manufacturing costs and utilization of many chemicals [1], thus leading to environmental degradation. A strategy that can replace these issues involves the use of abundantly available fish residues. Fish-derived HAp is easily obtainable through a simple process involving calcination [13,14] while serving as an economical and environmentally friendly source. It is also known for its higher calcium-phosphate content [15] and lower crystallinity [16] in comparison to the synthetically derived HAp [15]. These characteristics contribute towards higher surface reactivity *in-vivo* [17] and can be further improved by incorporating various dopants [16].

Herein, we describe the preparation of HAp from the fish scales of Tilapia (*Oreochromis niloticus*) and Catla (*Catla catla*) and compare it with the chemically synthesized. Further studies involve the preparation of NaCl-doped HAp, with a comprehensive evaluation of its physico-chemical characteristics. This co-substitution of Ca with Na and OH with Cl can make the HAp energetically unstable due to variations in electronegativity and ionic sizes, thus imparting them with improved *in-vivo* solubility. This, in turn, can lead to improved osseointegration capacity [16], which is relevant for bone tissue engineering.

2. Materials and Methods

2.1. Materials.

The chemicals utilized in the subsequent methodologies were of analytical grade. The scales for both fish varieties were obtained from the local market of Oman.

2.2. Methodology.

2.2.1. Preparation of undoped and doped synthetic hydroxyapatite.

The synthetic HAp, hereby referred to as ‘S’, was prepared chemically [18]. 0.5 M of calcium nitrate solution was added with 0.3 M ammonium phosphate solution dropwise, under continuous stirring at 90℃. The system’s pH was checked to 11.0 using ammonia solution, and the precipitate was washed through centrifugation. The precipitate was further dried at 120℃ and divided into two parts. One of the parts was doped with 5% NaCl, and then both doped and undoped parts were sintered at 800℃ for 2 hours to obtain the dry powder [18].

2.2.2. Preparation of undoped and doped hydroxyapatite from fish scales.

The fish scales from Tilapia and Catla were used to derive HAp. Scales from the two fish varieties were pre-processed by overnight soaking in distilled water. They were further soaked in 1 N HCl for 30 minutes to remove the protein content while subsequently increasing the pH to 11 with 6 N NaOH. The scales were then boiled in a water bath, and a part was doped with 5% NaCl. Both the parts were then placed at -80℃ for overnight freezing. They were further incubated at 160℃ and sintered at 800℃ for 2 hours to obtain the dry powder [18].

2.2.3. Characterization of synthetic and fish scale derived undoped and doped Hap.

The HAp obtained was studied for its physical characteristics by using electron microscopy and X-ray diffraction analysis. Samples S, T, and C (both doped and undoped) were placed over a clean stub using conductive carbon paint. The samples were completely dried and coated with platinum prior to their analysis by the Field Emission Scanning Electron Microscope, FESEM, JEOL (JSM-7600F). The surface morphology of all the sample types was further analyzed using ImageJ's image-processing software [19]. The 3-dimensional surface plots were constructed by first setting the scale (from the known distances) [20] and employing the pluggin' "Interactive 3D surface plot" [21]. Further, the average surface roughness of the samples was also determined by the prior elimination of background noise and light [20], followed by the utilization of the plugin "Roughness_calculation" [22]. The powdered HAp from all the sample types was used to study crystallinity through the PANalytical X, Pert Pro X-ray diffraction system. The measurements were performed by using Cu Kα radiations as the source of X-rays [23], keeping the 2θ range between 20 to 70° [24]. The 2θ peaks were compared with PDF-2 release 2012 (ICDD) and ICSD database for a comprehensive analysis. In addition, the elemental composition of the HAp samples was obtained through energy dispersive X-ray (EDX). The Fourier-Transform Infrared spectroscopy (Bruker ALPHA II spectrometer equipped with ATR) was further used at a scanning range of 400–4000 cm^{-1} to assess the presence of different chemical groups and their interactions. Finally, the Thermogravimetric analysis (TGA) and Differential Scanning calorimetry (DSC) were performed over a temperature range of 30-900°C and a heating rate of 10°C min^{-1}, using Perkin Elmer Pyris STA 6000. TGA was performed under atmospheric conditions to monitor the weight loss of all the HAp samples on encountering an increase in temperature, while DSC was carried out under a nitrogen atmosphere to determine their thermal transition point for melting or change in crystallinity.

3. Results and Discussions

The HAp was synthesized using chemical precursors and is further referred to as 'S', while that derived from Tilapia and Catala fish scales is labeled 'T' and 'C', respectively. The undoped and the doped HAp samples were thoroughly examined for their physical features through FESEM, as shown in Figures 1 and 2.

All the undoped samples revealed micro-scale architecture and the presence of densely packed HAp. Samples 'T' and 'C' comprised mixed morphologies of sticks, flakes, and particles when compared with 'S', which only had particle morphology. Such polygonal morphologies have also been described in some of the earlier reports [15,25,26], making it a characteristic feature of the HAp derived from fish scales. The samples also exhibited porous morphology. Samples 'S' and 'T' showed similar surface roughness values of 38.06 µm and 37.41µm, respectively, while for 'C', the surface was comparatively smoother (30.53 µm). This was also evident from the 3-dimensional surface plots of the undoped 'S', 'T', and 'C' (Figure 1). In comparison, the doped samples (Figure 2) revealed less density of HAp packing which can lead to improved interconnectivity [13]. The average surface roughness of 'T' and 'C' was enhanced after doping, while that of 'S' decreased a little (Table 1). It was evident that improved cell adhesion would follow among the doped samples, with 'T' presenting the best from among the group.

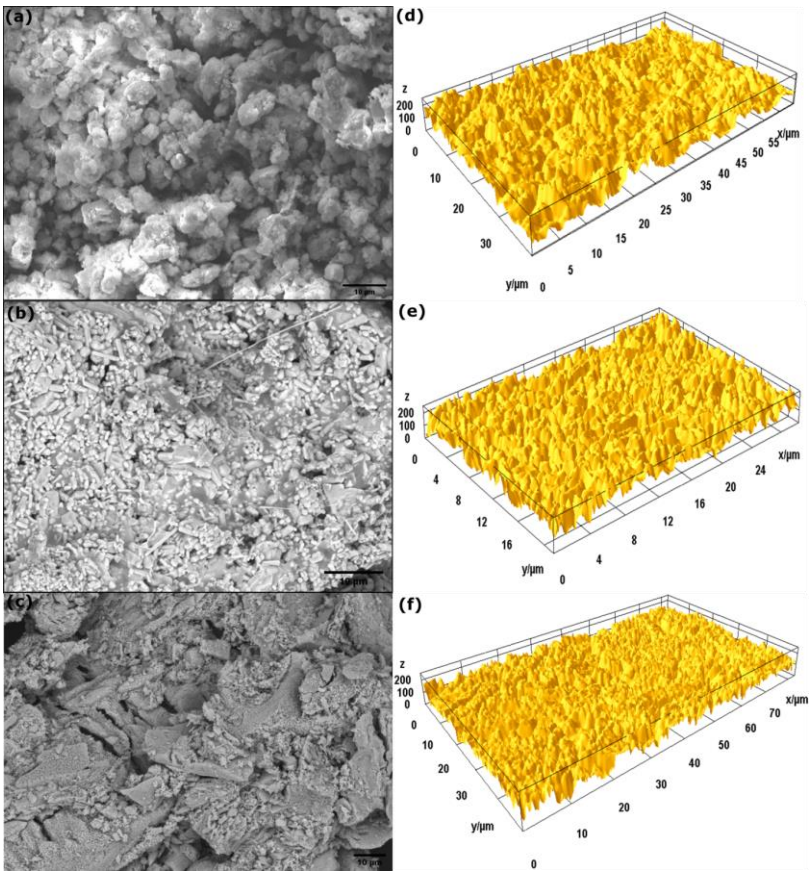

Figure 1. FESEM images of undoped **(a)** Synthetic HAp (S); **(b)** Tilapia derived (T); **(c)** Catla derived (C); with **(d), (e),** and **(f)** representing their 3-dimensional surface roughness plots respectively.

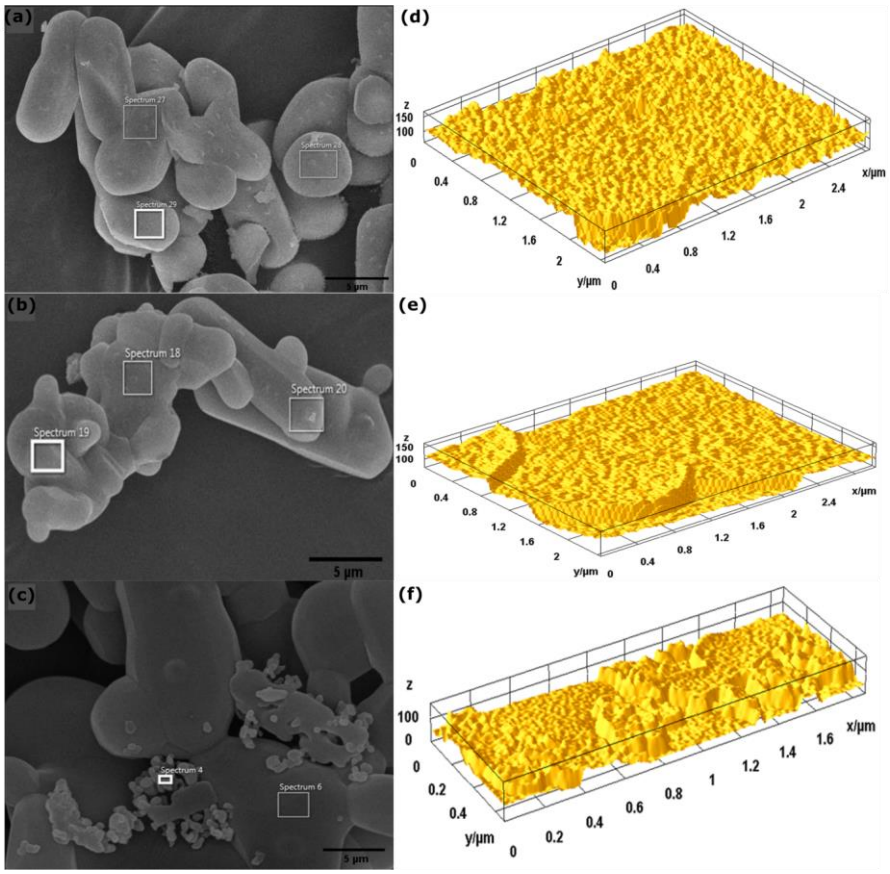

Figure 2. FESEM images of doped **(a)** Synthetic HAp (S); **(b)** Tilapia derived (T); **(c)** Catla derived (C); with **(d)**, **(e)**, and **(f)** representing their 3-dimensional surface roughness plots respectively.

Table 1. Average surface roughness values of undoped and doped S, T, and C Hap.

	Undoped			**Doped**		
HAp type	**S**	**T**	**C**	**S**	**T**	**C**
Average surface roughness (µm)	38.06	37.41	30.53	37.72	53.17	37.18

The elemental analysis for the doped sample types, 'T, and 'C' (Figure 3), showed the O, Ca, C, P, Al, Cl, and Na peaks, confirming the NaCl doping. The absence of N and S demonstrated the complete removal of the protein part while processing the fish scales, thus leading to the purity of the fish-derived HAp. The greater Ca/P ratios of 1.92 and 1.76 for 'T', and 'C', respectively, compared to the stoichiometric ratio of 1.67 generally obtained during chemical synthesis, are characteristic of the HAp derived from the fishes [15]. The Ca/P ratio exhibited by 'T' is similar to that found in normal human bones (1.9 to 2.1) [27], thus making it comparatively a more favorable choice than 'C'.

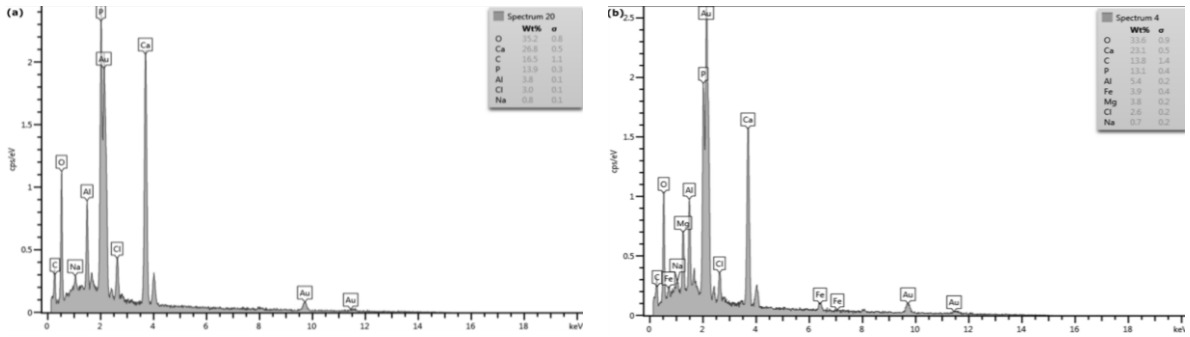

Figure 3. Elemental analysis of doped **(a)** Tilapia derived; **(b)** Catla derived Hap.

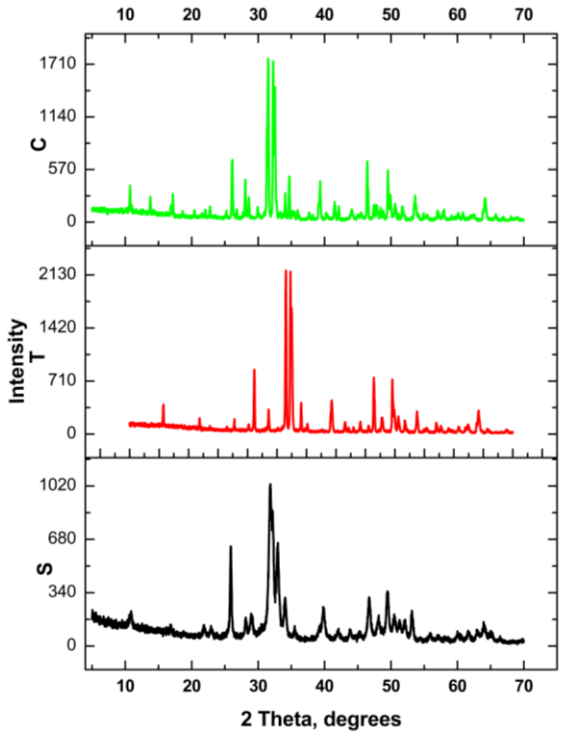

Figure 4. XRD spectrum of doped S, T, and C Hap.

The XRD analysis of doped, 'T', and 'C', depicted in Figure 4, revealed the prominent 2θ positions at 26°,32°,39°,49°, and 64°, which were similar in HAp extracted from bovine bone waste [28]. These also corresponded well with the 2θ values obtained with 'S', in comparison with the ICDD database- which provides primary and secondary peaks of HAp at

32.08° and 25.94°, respectively [15]. The absence of peak positions at 6°, 21°, or 33° also confirmed the absence of collagen protein [15], thus reinstating the results obtained in the elemental analysis.

The chemical features ascertained through FTIR measurements are shown in Figure 5. Undoped 'S' revealed the presence of hydroxyl, OH^- group at 3642 cm^{-1}, while the same was present at 3563 cm^{-1} for 'T' and 'C' [29,18]. This corresponded to the stretching and bending vibrations of the hydroxyl ions in the adsorbed water [25]. The asymmetric stretching vibration peaks of carbonates, CO_3^{2-} were confirmed by the bands at 1403 cm^{-1} for 'S' and 1461 cm^{-1} for 'T' and 'C'[15,30]. The v_3 vibration band of phosphate, PO_4^{3-} was centered about 1033 cm^{-1} for 'S', 'T', and 'C'[25]. Similarly, the bending vibrations of CO_3^{2-} and calcium the intense peaks at 872 cm-1 confirmed Ca^{2+} and 707 $cm^{-1,}$ respectively [25]. The absence of the amide bands further confirmed the purity of the developed scaffolds, as discussed earlier through EDX and XRD. The analysis of the doped samples revealed OH-Cl interactions at 3570 cm^{-1} and –HO: OH– 'head-on' configuration at 606 cm^{-1}, along with the other HAp peaks [16]. This suggested successful doping, as observed in the elemental analysis.

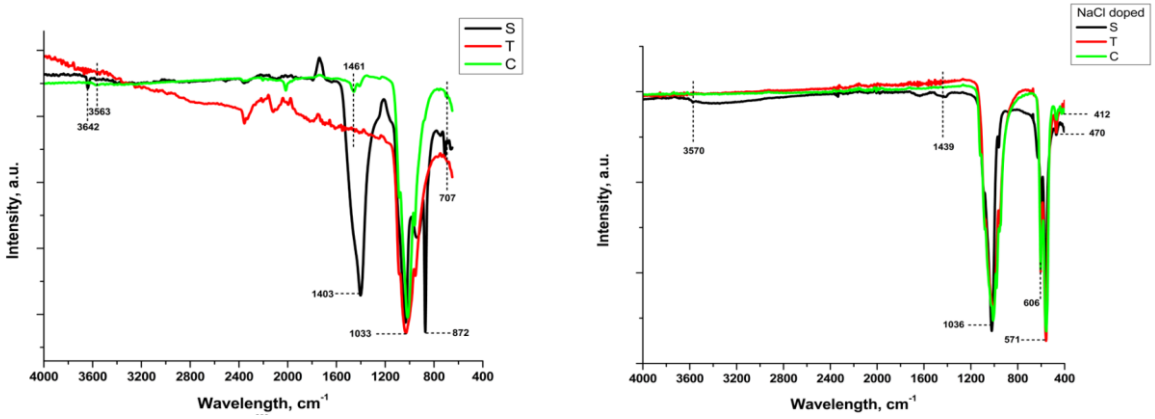

Figure 5. FTIR spectra of **(a)** undoped; **(b)** doped S, T, and C Hap.

Further, the undoped samples' thermal degradation behaviors (shown in Figure 6) revealed a few stages of weight loss. The first stage involved the evaporation of water and extended to around 390°C for sample 'S' while extending to about 275°C for 'T' and 'C'. In contrast, the doped 'S' showed around 5% weight loss till 200°C, while the samples 'T' and 'C' showed no significant weight loss over the entire temperature range extending to 900°C. The small amount of weight loss can be attributed to dehydration in the samples. The absence of other decomposition stages confirmed the purity of doped 'T' and 'C', hence proving their usability in the physiological temperature range.

The DSC analysis shown in Figure 7 indicates the better thermal stability of doped HAp than undoped HAp samples, even at temperatures above 5ºC. The thermal properties revealed with DSC provide the possibility of developing biomaterial applications with further processing and can be employed with acceptable physiological conditions.

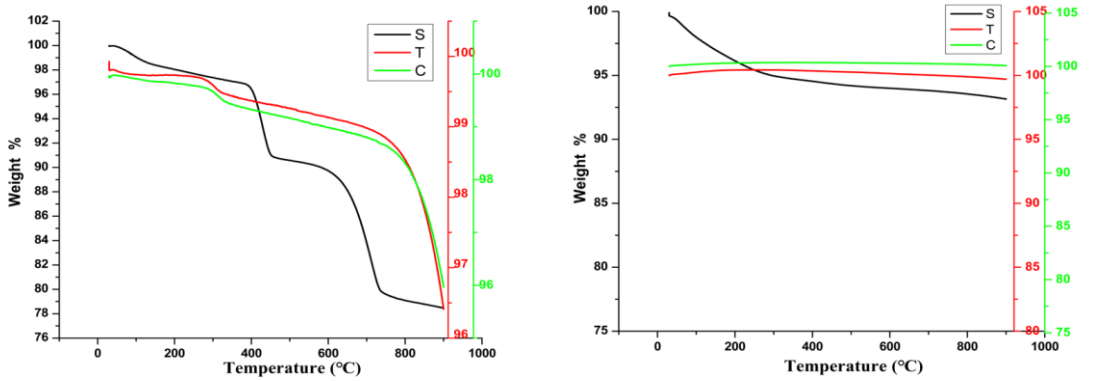

Figure 6. Thermal degradation studies of **(a)** undoped; **(b)** doped S, T, and C Hap.

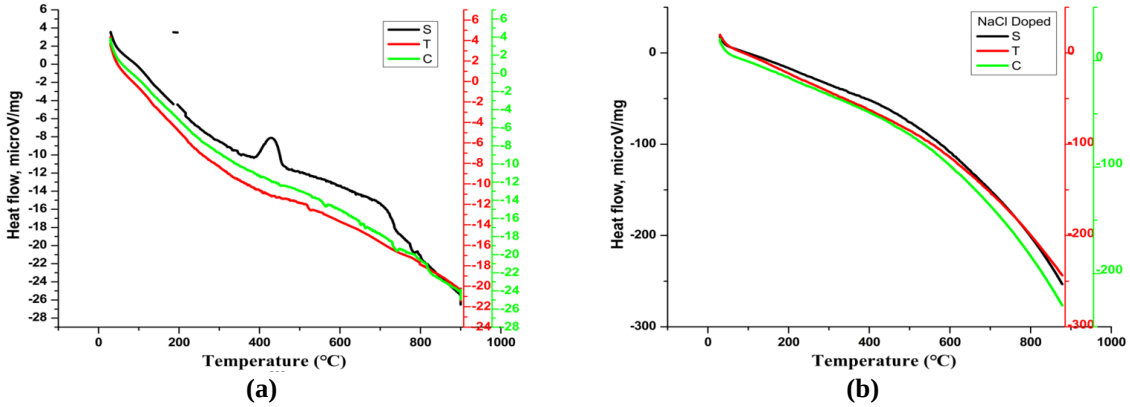

Figure 7. Differential Scanning calorimetry of **(a)** undoped; **(b)** doped S, T, and C Hap.

4. Conclusions and Future Perspectives

The present study showed the preparation of highly pure and crystalline HAp from Tilapia and Catla fish scales. The HAp obtained by removing the protein content and subsequent sintering at 800°C was further doped with 5% NaCl. Analysis of the physicochemical features revealed the formation of uniformly doped 'T' and 'C' HAp, thus rendering them with improved solubility, which is beneficial for tissue engineering applications. Better surface roughness values and Ca/P content for 'T' compared to 'C' indicate its better dispositioning for bone tissue regeneration, as this content plays a vital role in mineral homeostasis and bone metabolism. The development of porous scaffolds from the synthesized fish scale-derived doped HAp that supports osteoblast proliferation and the formation of extracellular matrix is desired in the future.

Funding

The study was funded by The Research Council (TRC), under the Ministry of Higher Education and Research & Innovation, Oman, for the category of Faculty Mentored Undergraduate Research Award Programme (FURAP), 2018-2019 cycle bearing the agreement number FURAP/CAS-SUR/18/011.

Acknowledgment

The authors thank the technical team of Mr. SaifAl-Mammari, Mr. Ahlam Al Azkawi, and Dr. S. Premkumar at Central Analytical & Applied Research Unit (CAARU), CAS, Sultan Qaboos University, Muscat, Oman, for their seamless support in analyzing the samples. The authors also forward their gratitude to the Deanship of the University of Technology and Applied Sciences-Sur, Oman, for all the support extended and for giving the Institutional Ethical clearance for this study. Further, Mr. Marwa Al Farsi, a lab technician, is the first to be affiliated with supporting analysis.

Conflict of Interest

The authors declare that they have no known competing financial or non-financial, professional, or personal conflicts that could have appeared to influence the work reported in this paper.

References

1. Granito, R.N.; Renno, A.C.; Yamamura, H.; de Almeida, M.C.; Menin Ruiz, P.L.; Ribeiro, D.A. Hydroxyapatite from Fish for Bone Tissue Engineering: A Promising Approach. *Int. J. Mol. Cell. Med.* **2018**, *7*, 80–90, https://doi.org/10.22088/IJMCM.BUMS.7.2.80.
2. Pon-On, W.; Suntornsaratoon, P.; Charoenphandhu, N.; Thongbunchoo, J.; Krishnamra, N.; Tang, I.M. Hydroxyapatite from fish scale for potential use as bone scaffold or regenerative material. *Mater. Sci. Eng. C* **2016**, *62*, 183–189, https://doi.org/10.1016/j.msec.2016.01.051.
3. Collins, M.N.; Ren, G.; Young, K.; Pina, S.; Reis, R.L.; Oliveira, J.M. Scaffold Fabrication Technologies and Structure/Function Properties in Bone Tissue Engineering. *Adv. Funct. Mater.* **2021**, *31*, 2010609, https://doi.org/10.1002/adfm.202010609.
4. Guo, L.; Liang, Z.; Yang, L.; Du, W.; Yu, T.; Tang, H.; Li, C.; Qiu, H. The role of natural polymers in bone tissue engineering. *J. Control. Release* **2021**, *338*, 571–582, https://doi.org/10.1016/j.jconrel.2021.08.055.
5. Alonzo, M.; Alvarez Primo, F.; Anil Kumar, S.; Mudloff, J.A.; Dominguez, E.; Fregoso, G.; Ortiz, N.; Weiss, W.M.; Joddar, B. Bone tissue engineering techniques, advances, and scaffolds for treatment of bone defects. *Curr. Opin. Biomed. Eng.* **2021**, *17*, 100248, https://doi.org/10.1016/j.cobme.2020.100248.
6. Aggarwal, A.; Sah, M.K. Chapter Three - Electrospun materials as scaffolds in tissue engineering and regenerative medicine. In Biomedical Applications of Electrospinning and Electrospraying, Kasoju, N., Ye, H., Eds.; Woodhead Publishing, **2021**; 83–121, https://doi.org/10.1016/B978-0-12-822476-2.00005-4.
7. Suamte, L.; Tirkey, A.; Barman, J.; Jayasekhar Babu, P. Various manufacturing methods and ideal properties of scaffolds for tissue engineering applications. *Smart Mater. Manuf.* **2023**, *1*, 100011, https://doi.org/10.1016/j.smmf.2022.100011.
8. Tang, G.; Liu, Z.; Liu, Y.; Yu, J.; Wang, X.; Tan, Z.; Ye, X. Recent Trends in the Development of Bone Regenerative Biomaterials. *Front. Cell Dev. Biol.* **2021**, *9*, 665813, https://doi.org/10.3389/fcell.2021.665813.
9. Shang, L.; Shao, J.; Ge, S. Immunomodulatory Properties: The Accelerant of Hydroxyapatite-Based Materials for Bone Regeneration. *Tissue Eng. Part C Methods* **2022**, *28*, 377–392, https://doi.org/10.1089/ten.tec.2022.00111112.
10. Shi, H.; Zhou, Z.; Li, W.; Fan, Y.; Li, Z.; Wei, J. Hydroxyapatite Based Materials for Bone Tissue Engineering: A Brief and Comprehensive Introduction. *Crystals* **2021**, *11*, 149, https://doi.org/10.3390/cryst11020149.
11. Rodríguez-Lugo, V.; Karthik, T.V.K.; Mendoza-Anaya, D.; Rubio-Rosas, E.; Villaseñor Cerón, L.S.; Reyes-Valderrama, M.I.; Salinas-Rodríguez, E. Wet chemical synthesis of nanocrystalline hydroxyapatite flakes: effect of pH and sintering temperature on structural and morphological properties. *R. Soc. Open Sci.* **2018**, *5*, 180962, https://doi.org/10.1098/rsos.180962.
12. Yelten-Yilmaz, A.; Yilmaz, S. Wet chemical precipitation synthesis of hydroxyapatite (HA) powders. *Ceram. Int.* **2018**, *44*, 9703–9710, https://doi.org/10.1016/j.ceramint.2018.02.201.

13. Deb, P.; Barua, E.; Deoghare, A.B.; Lala, S.D. Development of bone scaffold using *Puntius conchonius* fish scale derived hydroxyapatite: Physico-mechanical and bioactivity evaluations. *Ceram. Int.* **2019**, *45*, 10004–10012, https://doi.org/10.1016/j.ceramint.2019.02.044.
14. Deb, P.; Deoghare, A.B.; Barua, E. Poly ethylene glycol/fish scale-derived hydroxyapatite composite porous scaffold for bone tissue engineering. *IOP Conf. Ser. Mater. Sci. Eng.* **2018**, *377*, 012009, https://doi.org/10.1088/1757-899X/377/1/012009.
15. Liu, Y.; Liu, M.; Ji, S.; Zhang, L.; Cao, W.; Wang, H.; Wang, S. Preparation and application of hydroxyapatite extracted from fish scale waste using deep eutectic solvents. *Ceram. Int.* **2021**, *47*, 9366–9372, https://doi.org/10.1016/j.ceramint.2020.12.067.
16. Yoo, D.S.; Cho, J.S.; Chung, Y.-C.; Rhee, S.-H. Defect structures of sodium and chloride co-substituted hydroxyapatite and its osseointegration capacity. *J. Mater. Sci.* **2021**, *56*, 5493–5508, https://doi.org/10.1007/s10853-020-05645-9.
17. Um, S.-H.; Rhee, S.-H. *In vivo* evaluations of hydroxyapatites with small and large grain sizes. *Adv. Appl. Ceram.* **2019**, *118*, 484–490, https://doi.org/10.1080/17436753.2019.1667176.
18. Buraiki, N.S.S.A.; Ali Albadri, B.; Alsheriqi, S.; Alshabibi, B.; Al-Mammari, S.; Premkumar, S.; Sah, M.K.; Sudhakar, M.S. Characterization of *Catla catla* and *Oreochromis niloticus* fish scales derived hydroxyapatite scaffolds for regenerative medicine. *Mater. Today Proc.* **2020**, *27*, 2609–2616, https://doi.org/10.1016/j.matpr.2019.11.074.
19. Schneider, C.A.; Rasband, W.S.; Eliceiri, K.W. NIH Image to ImageJ: 25 years of image analysis. *Nat. Methods* **2012**, *9*, 671–675, https://doi.org/10.1038/nmeth.2089.
20. Aggarwal, A.; Sah, M.K. Process optimization for extraction of avian eggshell membrane derived collagen for tissue engineering applications. *J. Polym. Eng.* **2022**, *42*, 655-662, https://doi.org/10.1515/polyeng-2021-0315.
21. Interactive 3D Surface Plot Available online: https://imagej.nih.gov/ij/plugins/surface-plot-3d.html (accessed on 29 June 2022).
22. Chinga, G.; Johnsen, P.O.; Dougherty, R.; Berli, E.L.; Walter, J. Quantification of the 3D microstructure of SC surfaces. *J. Microsc.* **2007**, *227*, 254–265, https://doi.org/10.1111/j.1365-2818.2007.01809.x.
23. Shylaja, S.; Prashanthi, Y.; Nageswara Rao, T. Synthesis and evaluating the effects of nano hydroxyapatite on germination, growth and yield of cluster beans. *Mater. Today Proc.* **2022**, *64*, 917–921, https://doi.org/10.1016/j.matpr.2022.06.054.
24. Roopavath, U.K.; Sah, M.K.; Panigrahi, B.B.; Rath, S.N. Mechanochemically synthesized phase stable and biocompatible *β*-tricalcium phosphate from avian eggshell for the development of tissue ingrowth system. *Ceram. Int.* **2019**, *45*, 12910–12919, https://doi.org/10.1016/j.ceramint.2019.03.217.
25. Muhammad, N.; Gao, Y.; Iqbal, F.; Ahmad, P.; Ge, R.; Nishan, U.; Rahim, A.; Gonfa, G.; Ullah, Z. Extraction of biocompatible hydroxyapatite from fish scales using novel approach of ionic liquid pretreatment. *Sep. Purif. Technol.* **2016**, *161*, 129–135, https://doi.org/10.1016/j.seppur.2016.01.047.
26. Chinnappan, B.A.; Krishnaswamy, M.; Thanigachalam, M.; Xu, H.; Khan, S.I.; Hoque, M.E. Fabrication, Characterization and In Vitro Assessment of *Laevistrombus canarium*-Derived Hydroxyapatite Particulate-Filled Polymer Composite for Implant Applications. *Polymers* **2022**, *14*, 872, https://doi.org/10.3390/polym14050872.
27. Rollo, J.M.D.A.; Boffa, R.S.; Cesar, R.; Schwab, D.C.; Leivas, T.P. Assessment of Trabecular Bones Microarchitectures and Crystal Structure of Hydroxyapatite in Bone Osteoporosis with Application of the Rietveld Method. *Procedia Eng.* **2015**, *110*, 8–14, https://doi.org/10.1016/j.proeng.2015.07.003.
28. Han, K.-S.; Sathiyaseelan, A.; Saravanakumar, K.; Wang, M.-H. Wound healing efficacy of biocompatible hydroxyapatite from bovine bone waste for bone tissue engineering application. *J. Environ. Chem. Eng.* **2022**, *10*, 106888, https://doi.org/10.1016/j.jece.2021.106888.
29. Sharifi, S.; Zaheri Khosroshahi, A.; Maleki Dizaj, S.; Rezaei, Y. Preparation, Physicochemical Assessment and the Antimicrobial Action of Hydroxyapatite–Gelatin/Curcumin Nanofibrous Composites as a Dental Biomaterial. *Biomimetics* **2022**, *7*, 4, https://doi.org/10.3390/biomimetics7010004.
30. Dixit, K.; Kulanthaivel, S.; Agarwal, T.; Pal, K.; Giri, S.; Maiti, T.K.; Banerjee, I. Gum tragacanth modified nano-hydroxyapatite: An angiogenic- osteogenic biomaterial for bone tissue engineering. *Ceram. Int.* **2022**, *48*, 14672–14683, https://doi.org/10.1016/j.ceramint.2022.02.002.